Quantifying Total Superoxide, Peroxide and Carbonaceous Compounds in Metal-O_2 Batteries and the Solid Electrolyte Interface

Bettina Schafzahl,[†] Eléonore Mourad,[†] Lukas Schafzahl,[†] Yann K. Petit,[†] Anjana R. Raju,[†,‡] Musthafa Ottakam Thotiyl,[‡] Martin Wilkening,[†] Christian Slugovc,[†] Stefan A. Freunberger[†]*

[†]Institute for Chemistry and Technology of Materials, Graz University of Technology, Stremayrgasse 9, 8010 Graz, Austria

[‡]Department of Chemistry, Indian Institute of Science Education and Research (IISER) Pune, Dr. Homi Bhabha Road, Pashan, Pune, 411008, India

AUTHOR INFORMATION

Corresponding Author

* freunberger@tugraz.at

ABSTRACT Passivation layers on electrode materials are ubiquitous in nonaqueous battery chemistries and strongly govern performance and lifetime. They comprise break down products of the electrolyte including carbonate, alkyl carbonates, alkoxides, carboxylates and polymers. Parasitic chemistry in metal-O_2 batteries forms similar products and is tied to the deviation of the O_2 balance from the ideal stoichiometry during formation/decomposition of alkaline peroxides or superoxides. Accurate and integral quantification of carbonaceous species and peroxide or superoxide in battery electrodes remains, however, elusive. We present a refined procedure to quantify them accurately and sensitively by pointing out and rectifying pitfalls of previous procedures. Carbonaceous compounds are differentiated into inorganic and organic ones. We combine mass and UV-Vis spectrometry to quantify evolved O_2 and complexed peroxide, and CO_2 evolved from carbonaceous compounds by acid treatment and Fenton's reaction. The capabilities of the method are exemplified by means of Li–O_2 and Na–O_2 cathodes, graphite anodes and $LiNi_{0.8}Co_{0.15}Al_{0.05}O_2$ cathodes.

TOC GRAPHICS

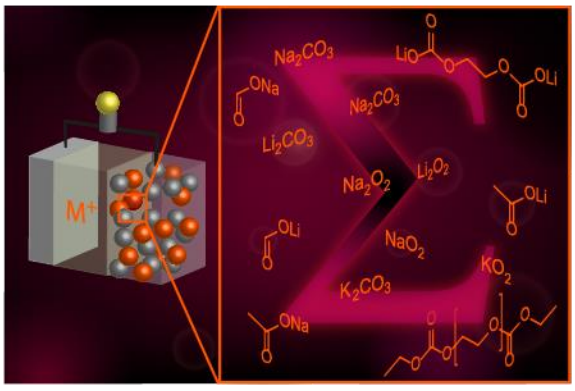

Lithium-ion batteries based on aprotic organic electrolytes store the highest energies of all current technologies due to the high operating potential. Nevertheless, society demands further improvements with respect to energy storage, cost, life time and materials sustainability.[1,2] Major routes to achieve these goals include advancing the currently used intercalation concept with higher-voltage cathodes[3,4] or replacing intercalation with higher-capacity conversion type electrodes such as the Si alloying anode[5,6] or the O_2 cathode[2,7], and analogous routes with Na^+ as the mobile ion.[8-13] In all cases, nature and quantity of parasitic chemistry with the electrolyte determines performance and lifetime.

Organic electrolytes decompose in contact with low voltage anode materials such as graphite or Si to form the solid electrolyte interphase (SEI).[14-22] Cathode materials equally get covered by such a layer – termed solid permeable interphase (SPI), especially so for materials with reactive surfaces or high redox voltages above 4.2 V.[23-25] These layers comprise break down products of the electrolyte solvent and salt including carbonate, alkyl carbonates, alkoxides, carboxylates and polymers (ethers and carbonates).[15-21,23-26] A large body of work over the last decades has identified mechanisms and parasitic products that form.[15-21,23-28] Accurate and integral quantification of these species, however, remains elusive.[29] Methods to identify the SEI/SPI components have been summarized in excellent reviews and include FTIR, XPS and NMR spectroscopy.[14-16,29,30] Li NMR and ICP-OES, for example, have been used to quantify Li at the interphase and total Li content.[30-32] However, Li content is not strictly tied to the overall interphase quantity as the compounds vary widely in Li-to-C ratio. Cell impedance is equally not directly linked to interphase quantity since the constituents contribute differently to impedance.[33,34] Total carbon content in the interphase would therefore be a key measure to assess.

Aprotic metal-O_2 cathodes store charge by forming/decomposing alkaline peroxides or superoxides.[2,7] Most typically these are Li peroxide (Li_2O_2), Na or K superoxide (NaO_2, KO_2), but also LiO_2, Na_2O_2 or mixtures of peroxide and superoxide were reported.[2,7,35-39] Albeit the reactions proceed at potentials within the electrochemical stability window of the electrolyte.[7] Reactive O_2 species, however, decompose electrolyte and carbon and form parasitic products including carbonates and carboxylates.[7,27,28,40-42] These carbonaceous compounds trap mobile ions, raise cell impedance, and cause capacity loss and cell failure.[2,7,14,15] Parasitic chemistry in O_2 cathodes is tied to the deviation of the O_2 balance from the ideal stoichiometry given by, e.g., $O_2 + 2Li^+ + 2e^- \leftrightarrow Li_2O_2$ and $O_2 + Na^+ + e^- \leftrightarrow NaO_2$, respectively. Concluding about the efficacy of measures to improve reversibility requires thus to relate the amount of peroxide or superoxide and the amount of parasitic products present to the charge passed.[40,43] However, known methods to measure these quantities feature significant inaccuracies.

Here we refine a previously reported method to more accurately quantify the total superoxide/peroxide and carbonaceous compounds in battery electrodes. We show that widely used methods for these quantities reported in the context of metal-O_2 batteries have pitfalls, which are prone to significant systematic errors and which we here clear out with refinements. Carbonaceous compounds are differentiated into inorganic and organic ones. We combine mass spectrometry (MS) and UV-Vis spectrometry to quantify evolved O_2 and complexed peroxide, and CO_2 evolved from carbonaceous compounds by acid treatment and Fenton's reaction. The capabilities of this refined method are exemplified by means of Li-O_2 and Na-O_2 cathodes, graphite anodes and $LiNi_{0.8}Co_{0.15}Al_{0.05}O_2$ cathodes.

Spectroscopic and diffractive methods sensitive to alkaline (su)peroxides or carbonaceous compounds such as XPS, FTIR, and XRD cannot quantify the integral amount in the electrode. To quantify them, the compounds may be chemically extracted and for consistency ideally quantified with a single sensitive method. The strategy we adopt here is to extract the compounds with aqueous solutions and to further digest them into O_2 and CO_2, which can then be quantified by mass spectrometry (MS). We first examine the possibility to measure the entire O_2 and CO_2 by MS. Since evolving all the O_2 from (su)peroxides turns out problematic, we combine MS and UV-Vis to quantify (su)peroxides. And we revisit and optimize our previously reported procedure to measure inorganic and organic carbon to also work in conjunction with the (su)peroxides measurement and for the SEI/SPI: treating the sample with acid evolves CO_2 from inorganic carbonate and semicarbonates, and treating with Fenton's reagent evolves CO_2 from organics.

Alkaline superoxides and peroxides (M = Li, Na, K, Rb, Cs) dissolve according to[44]

$$2\,MO_2 + 2\,H_2O \rightarrow H_2O_2 + O_2 + 2\,MOH \quad (1)$$

$$4\,MO_2 + 2\,H_2O \rightarrow 3O_2 + 4\,MOH \quad (2)$$

$$M_2O_2 + 2\,H_2O \rightarrow H_2O_2 + 2\,MOH \quad (3)$$

Recently, Wang et al. have shown that NaO_2 and KO_2 hydrolyze according to eq. 1 whereas LiO_2 follows eq. 2, which they could rationalize based on the reaction free energies. LiO_2 can thus not be quantified via the H_2O_2 formed.[36] We deal later on with the case that LiO_2 or mixtures of peroxide and superoxide are to be analyzed. Literature describes a range of methods to determine H_2O_2 including redox titration with I^-, MnO_4^-, and Ce^{4+} or photometric detection of Ti^{4+} or Co^{2+}–peroxo complexes.[45] A common pitfall is, however, that H_2O_2 is prone to decompose into H_2O and O_2, which underestimates the content. The reaction is particularly favored by catalytic surfaces, which are often used in metal-O_2 cells.[46] In the context of metal-O_2 batteries, H_2O_2 has

been quantified by 1) iodometric titration after immersing the electrode in H_2O and neutralizing with HCl[40] or 2) measuring the absorbance of the $[Ti(O_2)OH]^+$ complex after immersing the electrode in acidic $TiOSO_4$ solution.[38,44,47,48]

To test whether and how much these methods could underestimate the H_2O_2 by loss into the gas phase, we measured the evolved O_2 by MS during the immersion steps, Fig. 1. The setup consisted of a hermetically sealed glass vial equipped with a stirring bar and a lid with septum and tubing for purge gas, Fig. S1. The gas space was continuously purged into a MS for gas analysis. To resemble major electrode types we tested next to pure Li_2O_2 also mechanical mixtures of Li_2O_2 with carbon black and a mixture with additional α-MnO_2.

Turning first to the preparation for titration, immersing pure Li_2O_2 in H_2O evolves O_2 at somewhat fading rate after an initial peak, Fig. 1a. Once acid is added O_2 evolution rises again to fade thereafter quickly to the base line. With the Li_2O_2/C mixture, O_2 evolves at a higher, nearly constant rate and also drops once acid is added. The O_2 amounts equate to ~3 and 8%, respectively, of the H_2O_2. With the Li_2O_2/C/MnO_2 mixture, O_2 evolves at initially ~400 times the previous rate to quantitatively evolve all O_2 within ~300 s. Turning to the preparation for Ti^{4+} photometry, Fig. 1b, immersing pure Li_2O_2, Li_2O_2/C or Li_2O_2/C/MnO_2 mixtures leads to O_2 evolution in the same order as before. The O_2 amounts equate to 0.3, 7, and 55% of the total peroxide, respectively. Fast catalytic decomposition of H_2O_2 by transition metal oxides is in accord with its use to probe catalytic activity[46] and renders measuring H_2O_2 by titration or photometry alone impracticable for electrodes with catalysts. The results also show that significant amounts of H_2O_2 can be lost with only marginally catalyzing C surfaces and even with pure Li_2O_2. Similarly, immersing NaO_2 or KO_2 in water or acid releases more O_2 than

commensurate with Eq. 1, which indicates significant decomposition of the formed H_2O_2, Table 1.

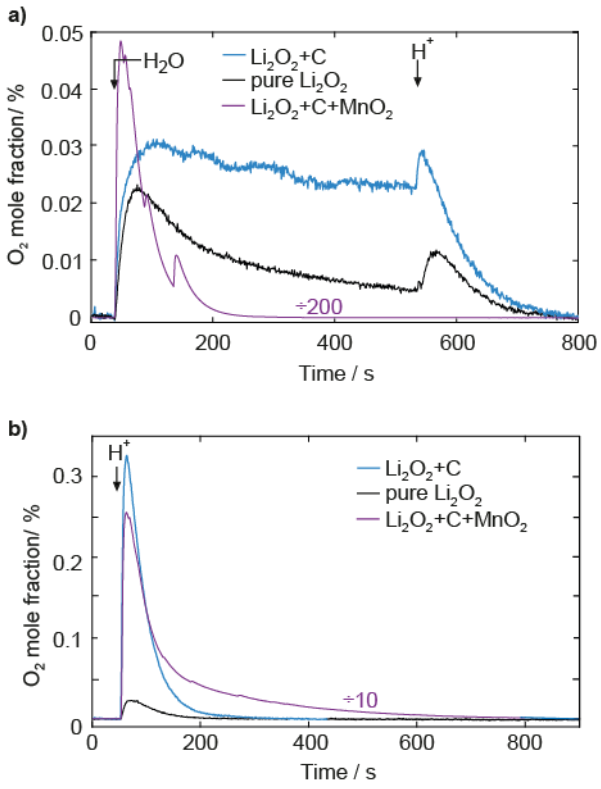

Figure 1. Oxygen loss into the gas phase upon sample preparation for peroxide/superoxide detection by titration (a) or photometry (b). The samples are pure Li_2O_2 and mechanical mixtures of Li_2O_2 with SuperP carbon (1:1) and Li_2O_2 with SuperP carbon and α-MnO_2 (1:0.6:0.4), which mimic discharged Li–O_2 cathodes without and with catalyst. Iodometric titration involves adding water and then acid and is analyzed in (a). Photometry involves adding $TiOSO_4$ in 0.1 M H_2SO_4 solution and is analyzed in (b).

Table 1. Amount of released O_2 with respect to the NaO_2 or KO_2 amount when immersed in water or acid. Note that for every mol O_2 two mol H_2O_2 are decomposed. For NaO_2 Na-O_2 cathodes discharged in 0.5 M NaOTf in diglyme containing 40 ppm H_2O were used. For KO_2 commercial material was used. The total NaO_2 or KO_2 amount was determined by combining MS and UV-Vis measurements.

	O_2/NaO_2	O_2/KO_2
ideal	0.5	0.5
immersed in H_2O	0.554	0.523
immersed in 0.1 M H_2SO_4	0.520	0.528
immersed in 1 M H_2SO_4	0.525	0.557

Measuring O_2 from peroxide/superoxide by evolving it into the gas phase appears an attractive option given the described significant O_2 evolution. Prerequisite is to evolve O_2 quantitatively and to avoid reactive O_2 species, which could decompose organics into CO_2. The latter would not allow distinguishing CO_2 from organics and inorganics as intended and underestimate the peroxide/superoxide amount. Although effective in decomposing H_2O_2, transition metal oxides do form reactive species and prematurely decompose organics, Fig. S2a. H_2O_2 may, however, also catalytically be decomposed by Fe^{3+} for which either the Kremer-Stein mechanism[44] or other mechanisms involving $HO_2^{\bullet}$ or $^{\bullet}OH$ were proposed.[49] Fe^{3+} quantitatively decomposes all H_2O_2, Table S1 and Fig. S3. When, however, Li acetate was added as a probe for reactive species the sample evolved CO_2 (Fig. S2b), indicating a pathway with reactive species[49]. Overall, quantifying superoxide and peroxide by evolving them as O_2 is problematic as reactive oxygen species form, which causes O_2 to be underestimated and organic carbon to be falsely assigned as inorganic.

Superoxide and peroxide may thus best be quantified by combining photometry of the $[Ti(O_2)OH]^+$ complex and MS measurement of the O_2 evolved during sample preparation. In the case that electrodes containing only peroxides are measured, the O_2 comprises O_2 from H_2O_2 decomposition. In the case of superoxides the O_2 comprises the O_2 from quantitative disproportionation according to eq. 1 and additional O_2 from H_2O_2 decomposition (except for LiO_2, which does not form H_2O_2). The total moles *n* of M_2O_2 or MO_2 (M = Li, Na, K) are obtained via

$$n_{M_2O_2} = n_{H_2O_2} + 2 \cdot n_{O_2} \text{ , M = Li, Na, K} \quad (4)$$

$$n_{LiO_2} = \frac{3}{4} n_{O_2} \quad (5)$$

$$n_{MO_2} = \frac{4}{3}\left(n_{O_2} + \frac{1}{2} \cdot n_{H_2O_2}\right) \text{ , M = Na, K} \quad (6)$$

These equations are derived in the Supplementary Discussion and Fig. S4. In some cases it was shown that Li-O_2 and Na-O_2 cells can yield mixtures of superoxide and peroxide as discharge product.[35-39,48] When mixtures are to be expected, determining the individual amounts requires additionally to measure the moles *n* of Li^+ or Na^+ as discussed in the Supplementary Discussion and Fig. S5. The total moles *n* of M_2O_2 and MO_2 are obtained via

$$\boldsymbol{n_{Li_2O_2} = \frac{6}{13}\left(\frac{4}{3} n_{Li^+} - \frac{1}{2} n_{H_2O_2} - n_{O_2}\right)} \quad (7)$$

$$\boldsymbol{n_{LiO_2} = n_{Li^+} - 2 n_{Li_2O_2}} \quad (8)$$

for Li_2O_2 and LiO_2 mixtures and

$$\boldsymbol{n_{Na_2O_2} = \frac{3}{4} n_{Na^+} - \frac{1}{2} n_{H_2O_2} - n_{O_2}} \quad (9)$$

$$\boldsymbol{n_{NaO_2} = n_{Na^+} - 2 n_{Na_2O_2}} \quad (10)$$

for Na_2O_2 and NaO_2 mixtures.

Calibrating UV-Vis absorbance with H_2O_2 is prone to yield a curve that does not pass through zero, i.e. due to loss of H_2O_2.[38] To obtain the true H_2O_2 concentration, we thus started from high purity Li_2O_2 and accounted for any H_2O_2 loss by measuring evolved O_2, Fig. S6.

Fenton's reaction, which forms the highly reactive $^{\bullet}OH$ radical via $Fe^{2+} + H_2O_2 \rightarrow Fe^{3+} + OH^- + {}^{\bullet}OH$, is used to decompose organics into CO_2 and proceeds best at a pH of 3,[50] while peroxide/superoxide analysis is ideal at more acidic condition (compare Fig. 1b vs. Fig. 2d). To quantify peroxide/superoxide and carbonaceous compounds in combination, the optimized procedure for sample sizes of several mg, which are typically used in coin cells or Swagelok type cells is shown in Fig. 2. The procedure for metal–O_2 electrodes is summarized in Fig. 2b, the procedure for all other electrodes in Fig. 2c. The first involves as first step acidifying the sample with 1 M H_2SO_4 upon which CO_2 evolves from M_2CO_3. The strongly acidic pH prevents excessive O_2 evolution from H_2O_2. To quantify the dissolved peroxide, after CO_2 and O_2 evolution have ceased, part of the solution is removed and mixed with $TiOSO_4$ solution and analyzed by UV-Vis. The remaining solution in the MS setup is then diluted with H_2O to reach the optimum pH of 3. Fenton's reaction is then initiated by adding $FeSO_4$ in 0.1 M H_2SO_4 and then, over the course of several minutes, H_2O_2 in 0.1 M H_2SO_4 under vigorous stirring. For electrodes other than metal-O_2 cathodes the first step is modified by adding a smaller amount of 1 M H_2SO_4, Fig. 2c. Samples that contain alkylcarbonates ($ROCO_2M$) such as in the SEI or the SPI evolve CO_2 according to $ROCO_2M + H_2O \rightarrow ROH + MOH + CO_2$. Successive treatment with acid and Fenton's reagent can quantitatively discriminate between CO_2 from M_2CO_3 or the terminal $–OCO_2M$ groups of $ROCO_2M$ and CO_2 from organic moieties. Table 2 compares expected and evolved moles of CO_2 for a range of compounds including Li_2CO_3, Li acetate and different Li alkylcarbonates. In all cases the values match the expected values within 3% and

confirm the reagents to expel the compounds selectively and quantitatively. Further on we refer to inorganic CO_2 when evolving from acid and organic CO_2 when evolving from Fenton's reaction.

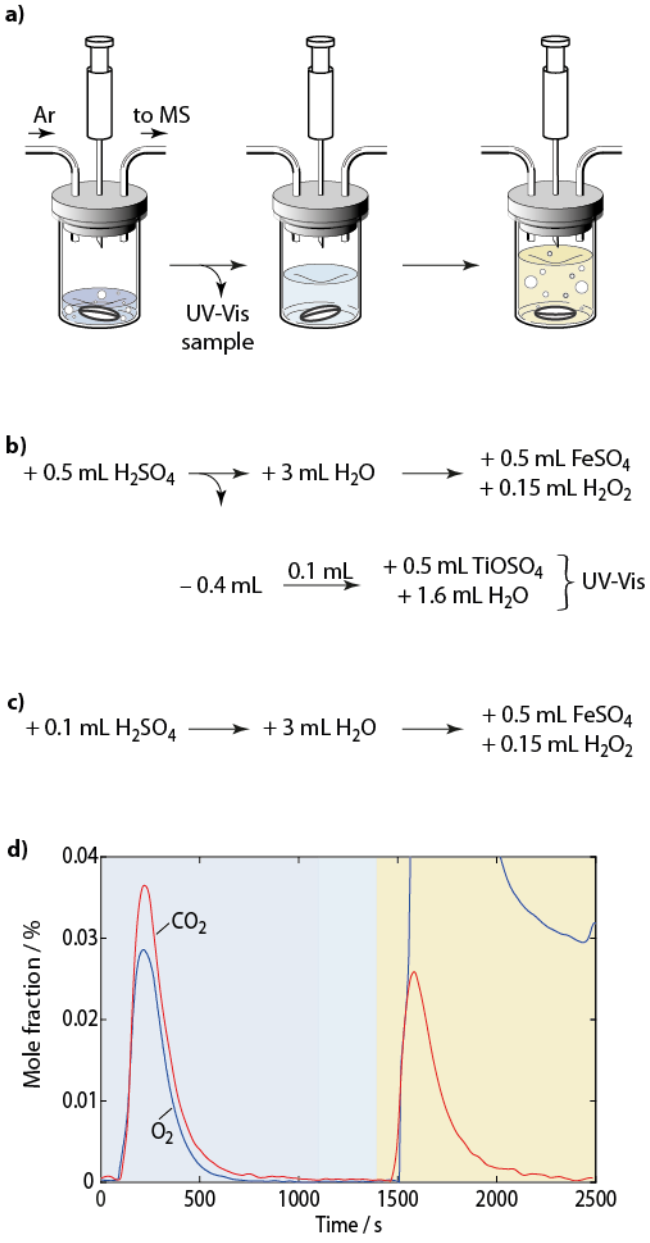

Figure 2. Analysis protocol to quantify total superoxide/peroxide and carbonaceous products in battery electrodes. a) Schematic of the test setup and the sequence of solution addition and sample drawing. b) Procedure for metal-O_2 cathodes. The concentrations in the added solutions

are 1 M H_2SO_4, 0.5 M $FeSO_4$ in 0.1 M H_2SO_4, 10 wt% H_2O_2 in 0.1 M H_2SO_4, and 2 wt% $TiOSO_4$ in 1 M H_2SO_4, respectively. Quantification of total superoxide/peroxide by combining O_2 detected by MS and H_2O_2 by UV-Vis photometry is detailed in the Supplementary Discussion and Figs. S5 and S6. c) Procedure for electrodes other than metal-O_2. d) CO_2 and O_2 evolution during the course of a typical analysis. In the particular case a discharged Li–O_2 cathode was measured. The color coded background refers to the stages indicated in (a). CO_2 during the blue period stems from inorganic carbonates or terminal –OCO_2Li groups in alkyl carbonates; CO_2 during the yellow shaded period evolves from organics being oxidized by Fenton's reaction.

Table 2. Expected and measured moles of CO_2 evolved per mol of Li_2CO_3, Li acetate and Li alkylcarbonates. Inorganic refers to CO_2 evolved from acid treatment, organic to CO_2 evolved from Fenton's reagent.

	expected		found	
compound	inorganic	organic	inorganic	organic
Li_2CO_3 [1)]	1	-	1±0.03	-
CH_3COOLi [1)]	-	2	-	2±0.01
CH_3OCO_2Li	1	1	1±0.02	1±0.02
$CH_3(CH_2)_3OCO_2Li$	1	4	1±0.02	4±0.04

[1)] A curve for the found vs. the expected amount is given in Fig. S7.

Figure 2d shows a typical concentration profile for O_2 and CO_2 during the analysis of a Li–O_2 cathode. For the particular cell the presented method gives a Li_2O_2 yield of 94% (based on the expected amount with respect to the charge passed), while UV-Vis measurement alone after immersing the electrode in 2% $TiOSO_4$ in 0.1M H_2SO_4 gave a yield of only 85%. Figure S8 shows a typical measurement of a Na–O_2 cathode. The optimized method gave a yield of 96%

whereas UV-Vis alone gave ~94% NaO_2 yield. Figure 3 shows the values obtained with the optimized method over an entire discharge and charge cycle of a Li-O_2 and Na-O_2 cell.

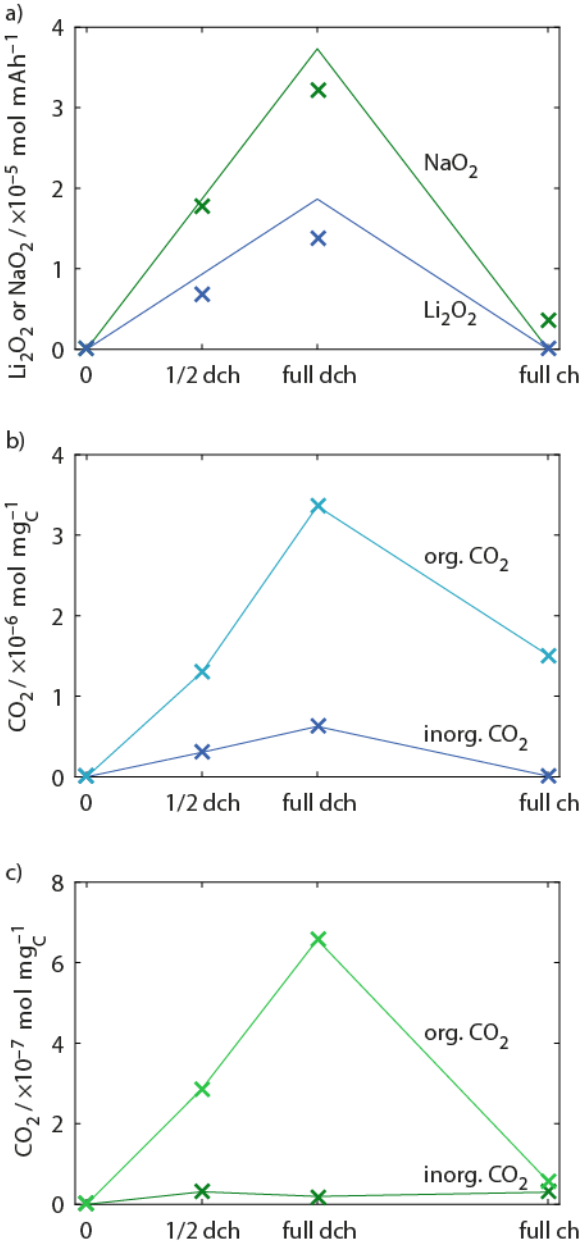

Figure 3. Product quantification over an entire discharge/charge cycle of a Li-O_2 and Na-O_2 cell determined at half and full discharge and full charge (labeled 1/2 dch, full dch, full ch, respectively). Li-O_2 cells comprised a Super P/PTFE working electrode, $Li_{1-x}FePO_4$ reference and counter electrodes and 0.1 M $LiClO_4$ in tetraglyme as the electrolyte and were run at 70

$mA \cdot g_C^{-1}$ with full discharge corresponding to 1200 $mAh \cdot g_C^{-1}$. Na-O_2 cells comprised a carbon paper working electrode, Na metal reference and counter electrodes and 0.1 M NaOTf in diglyme containing 40 ppm H_2O as the electrolyte and were run at 90 $\mu A \cdot cm^{-2}$ with full discharge corresponding to 1 $mAh \cdot cm^{-2}$. Markers represent the measured amounts of Li_2O_2 and NaO_2, respectively, and full lines the theoretical values. b) Amounts of inorganic and organic CO_2 at the sampling points for the Li-O_2 cell. c) Amounts of inorganic and organic CO_2 at the sampling points for the Li-O_2 cell. The first sampling point is in either case the electrode brought in contact with electrolyte overnight. Electrodes were washed with dimethoxyethane and dried under vacuum prior to analysis.

Figure 4 exemplifies the capabilities of the method to follow SEI/SPI evolution on graphite anodes and $LiNi_{0.8}Co_{0.15}Al_{0.05}O_2$ cathodes. The electrodes were cycled vs. Li-metal in LP30 electrolyte to various stages of charge, then stopped and analyzed. Electrodes were either washed with dimethyl carbonate or used unwashed to capture the difference the washing introduces. It is a known problem for interphase analytics that washing is at the one hand required for surface sensitive methods such as XPS but on the other hand may alter the interphase composition. Unwashed electrodes were only analyzed for inorganic CO_2, capturing M_2CO_3 and terminal –OCO_2M groups of alkylcarbonates, since Fenton's reagent would decompose the electrolyte.

Considering first the initial lithiation of graphite, inorganic CO_2 in the unwashed electrodes continuously grows to full lithiation, Fig. 4a. Values for inorganic and organic CO_2 from the washed electrodes show, in contrast, a pronounced maximum at half lithiation and decrease to full lithiation. Multiple measurements at half lithiation confirm the values to be statistically significant. To interpret this behavior it needs to be recalled what the values represent. Organic CO_2 captures all organic compounds not washed away by dimethyl carbonate. These may not

only comprise Li-containing ones but also oligo carbonates, oligo ethylene oxides, carbonate terminated ethylene oxides, and remaining electrolyte.[19-21,26] Declining amounts from half to full lithiation may be explained along the reaction schemes described by Gachot et al. by ongoing reactions triggered by CH_3OLi, which breaks initially present oligo carbonates into the more soluble oligo ethylene oxides and CH_3OCO_2Li.[19] These reactions not only take place directly on the graphite surface but in a distance such as in the separator. Conversion into more soluble or poorly attached species is also suggested by the trend of the inorganic CO_2 beyond the first lithiation in the unwashed electrodes, which captures both Li_2CO_3, terminal $–OCO_2Li$ groups and soluble compounds. Another feature seen in the washed electrodes is a tendency for higher/lower amounts in the lithiated/delithiated states, which is in accord with dynamic change in SEI thickness noted earlier by Edström et al.[22] A more detailed analysis of the underlying phenomena is, however, beyond the scope of this study, which is concerned with the method itself. As another example we measured the SPI evolution on NCA cathodes, Fig. 4c. Inorganic CO_2 in slightly lower in the washed compared to unwashed electrodes and remains at nearly the same level without clear evolution. The main constituents in quantitative terms are organic compounds, which grow with cycle number and correlate well with the growing efficiency.

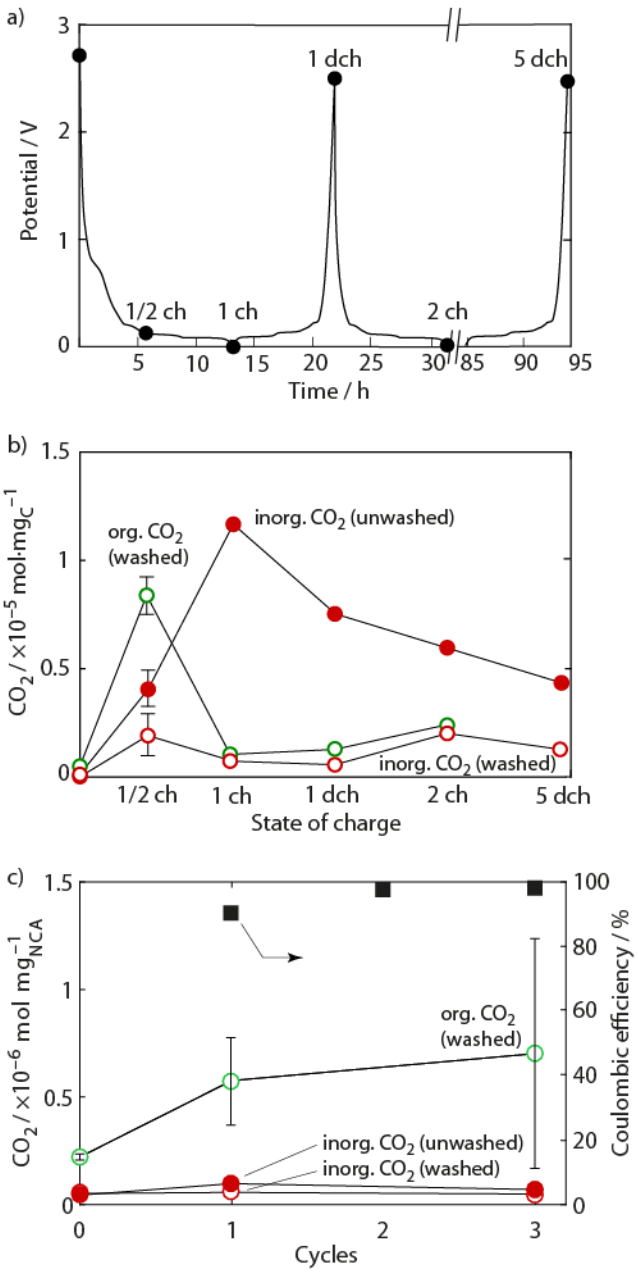

Figure 4. The evolution of total carbonaceous SEI and SPI components. The first sampling point is in either case the electrode brought in contact with electrolyte overnight. Electrodes were either washed with dimethyl carbonate prior to analysis or analyzed unwashed to capture soluble SEI components. Washed electrodes were analyzed with acid and Fenton's reaction for inorganic and organic CO_2; unwashed electrodes were analyzed only with acid. a) Voltage versus time during cycling of a graphite anode in LP30 electrolyte with the sampling points indicated by the

black markers. b) Amount of CO_2 found at the sampling points. c) Evolution of coulombic efficiency and total carbonaceous SPI components during cycling of a $LiNi_{0.8}Co_{0.15}Al_{0.05}O_2$ cathode in LP30 electrolyte. The error bars are derived from at least three measurements.

In conclusion we present a refined method to accurately and sensitively quantify total superoxide or peroxide and carbonaceous compounds in battery electrodes. The method for peroxide and superoxide clears out pitfalls with uncontrolled O_2 loss into the gas phase, which makes previously reported methods prone to underestimated values. Carbonaceous compounds are differentiated into inorganic and organic ones and the measures can discriminate between soluble and insoluble compounds by comparing washed and unwashed electrodes.

ASSOCIATED CONTENT

Supporting Information. Materials, experimental methods, supporting figures and discussion.

AUTHOR INFORMATION

Corresponding Author

*E-mail: freunberger@tugraz.at

web: www.freunberger-lab.com

Notes

The authors declare no competing financial interest.

ACKNOWLEDGMENT

S.A.F. is indebted to the European Research Council (ERC) under the European Union's Horizon 2020 research and innovation programme (grant agreement No 636069) and the Austrian Federal Ministry of Science, Research and Economy and the Austrian Research Promotion Agency (grant No. 845364).

REFERENCES

(1) Larcher, D.; Tarascon, J. M. Towards Greener and More Sustainable Batteries for Electrical Energy Storage. *Nat. Chem.* **2014**, *7*, 19–29.

(2) Choi, J. W.; Aurbach, D. Promise and Reality of Post-Lithium-Ion Batteries with High Energy Densities. *Nat. Rev. Mater.* **2016**, *1*, 16013.

(3) Brutti, S.; Greco, G.; Reale, P.; Panero, S. Insights About the Irreversible Capacity of $LiNi_{0.5}Mn_{1.5}O_4$ Cathode Materials in Lithium Batteries. *Electrochim. Acta* **2013**, *106*, 483-493.

(4) Xu, M.; Lu, D.; Garsuch, A.; Lucht, B. L. Improved Performance of $LiNi_{0.5}Mn_{1.5}O_4$ Cathodes with Electrolytes Containing Dimethylmethylphosphonate (DMMP). *J. Electrochem. Soc.* **2012**, *159*, A2130-A2134.

(5) Obrovac, M. N.; Chevrier, V. L. Alloy Negative Electrodes for Li-Ion Batteries. *Chem. Rev.* **2014**, *114*, 11444-11502.

(6) Chevrier, V. L.; Ceder, G. Challenges for Na-Ion Negative Electrodes. *J. Electrochem. Soc.* **2011**, *158*, A1011-A1014.

(7) Aurbach, D.; McCloskey, B. D.; Nazar, L. F.; Bruce, P. G. Advances in Understanding Mechanisms Underpinning Lithium–Air Batteries. *Nat. Energy* **2016**, *1*, 16128.

(8) Kim, S.-W.; Seo, D.-H.; Ma, X.; Ceder, G.; Kang, K. Electrode Materials for Rechargeable Sodium-Ion Batteries: Potential Alternatives to Current Lithium-Ion Batteries. *Adv. Energy Mater.* **2012**, *2*, 710-721.

(9) Slater, M. D.; Kim, D.; Lee, E.; Johnson, C. S. Sodium-Ion Batteries. *Adv. Funct. Mater.* **2013**, *23*, 947-958.

(10) Ellis, B. L.; Nazar, L. F. Sodium and Sodium-Ion Energy Storage Batteries. *Curr. Opin. Solid State Mater. Sci.* **2012**, *16*, 168-177.

(11) Ponrouch, A.; Marchante, E.; Courty, M.; Tarascon, J.-M.; Palacin, M. R. In Search of an Optimized Electrolyte for Na-Ion Batteries. *Energy Environ. Sci.* **2012**, *5*, 8572-8583.

(12) Wu, D.; Li, X.; Xu, B.; Twu, N.; Liu, L.; Ceder, G. $NaTiO_2$: A Layered Anode Material for Sodium-Ion Batteries. *Energy Environ. Sci.* **2015**, *8*, 195-202.

(13) Clément, R. J.; Bruce, P. G.; Grey, C. P. Manganese-Based P2-Type Transition Metal Oxides as Sodium-Ion Battery Cathode Materials. *J. Electrochem. Soc.* **2015**, *162*, A2589-A2604.

(14) Xu, K. Nonaqueous Liquid Electrolytes for Lithium-Based Rechargeable Batteries. *Chem. Rev.* **2004**, *104*, 4303-4418.

(15) Xu, K. Electrolytes and Interphases in Li-Ion Batteries and Beyond. *Chem. Rev.* **2014**, *114*, 11503–11618.

(16) Verma, P.; Maire, P.; Novák, P. A Review of the Features and Analyses of the Solid Electrolyte Interphase in Li-Ion Batteries. *Electrochim. Acta* **2010**, *55*, 6332-6341.

(17) Eshetu, G. G.; Grugeon, S.; Kim, H.; Jeong, S.; Wu, L.; Gachot, G.; Laruelle, S.; Armand, M.; Passerini, S. Comprehensive Insights into the Reactivity of Electrolytes Based on Sodium Ions. *ChemSusChem* **2016**, 462–471.

(18) Kim, H.; Grugeon, S.; Gachot, G.; Armand, M.; Sannier, L.; Laruelle, S. Ethylene Bis-Carbonates as Telltales of SEI and Electrolyte Health, Role of Carbonate Type and New Additives. *Electrochim. Acta* **2014**, *136*, 157-165.

(19) Gachot, G.; Grugeon, S.; Armand, M.; Pilard, S.; Guenot, P.; Tarascon, J.-M.; Laruelle, S. Deciphering the Multi-Step Degradation Mechanisms of Carbonate-Based Electrolyte in Li Batteries. *J. Power Sources* **2008**, *178*, 409-421.

(20) Gireaud, L.; Grugeon, S.; Laruelle, S.; Pilard, S.; Tarascon, J.-M. Identification of Li Battery Electrolyte Degradation Products through Direct Synthesis and Characterization of Alkyl Carbonate Salts. *J. Electrochem. Soc.* **2005**, *152*, A850-A857.

(21) Sasaki, T.; Abe, T.; Iriyama, Y.; Inaba, M.; Ogumi, Z. Formation Mechanism of Alkyl Dicarbonates in Li-Ion Cells. *J. Power Sources* **2005**, *150*, 208-215.

(22) Bryngelsson, H.; Stjerndahl, M.; Gustafsson, T.; Edström, K. How Dynamic Is the SEI? *J. Power Sources* **2007**, *174*, 970-975.

(23) Philippe, B.; Hahlin, M.; Edström, K.; Gustafsson, T.; Siegbahn, H.; Rensmo, H. Photoelectron Spectroscopy for Lithium Battery Interface Studies. *J. Electrochem. Soc.* **2016**, *163*, A178-A191.

(24) Younesi, R.; Christiansen, A. S.; Scipioni, R.; Ngo, D.-T.; Simonsen, S. B.; Edström, K.; Hjelm, J.; Norby, P. Analysis of the Interphase on Carbon Black Formed in High Voltage Batteries. *J. Electrochem. Soc.* **2015**, *162*, A1289-A1296.

(25) Edström, K.; Gustafsson, T.; Thomas, J. O. The Cathode–Electrolyte Interface in the Li-Ion Battery. *Electrochim. Acta* **2004**, *50*, 397-403.

(26) Gireaud, L.; Grugeon, S.; Pilard, S.; Guenot, P.; Tarascon, J.-M.; Laruelle, S. Mass Spectrometry Investigations on Electrolyte Degradation Products for the Development of Nanocomposite Electrodes in Lithium Ion Batteries. *Anal. Chem.* **2006**, *78*, 3688-3698.

(27) McCloskey, B. D.; Bethune, D. S.; Shelby, R. M.; Girishkumar, G.; Luntz, A. C. Solvents' Critical Role in Nonaqueous Lithium–Oxygen Battery Electrochemistry. *J. Phys. Chem. Lett.* **2011**, *2*, 1161-1166.

(28) Ottakam Thotiyl, M. M.; Freunberger, S. A.; Peng, Z.; Bruce, P. G. The Carbon Electrode in Nonaqueous Li–O_2 Cells. *J. Am. Chem. Soc.* **2013**, *135*, 494-500.

(29) Lu, J.; Wu, T.; Amine, K. State-of-the-Art Characterization Techniques for Advanced Lithium-Ion Batteries. *Nat. Energy* **2017**, *2*, 17011.

(30) Dupré, N.; Cuisinier, M.; Guyomard, D. Electrode-Electrolyte Interface Studies in Lithium Batteries Using Nmr. *ECS Interface* **2011**, *20*, 61-67.

(31) Schwieters, T.; Evertz, M.; Mense, M.; Winter, M.; Nowak, S. Lithium Loss in the Solid Electrolyte Interphase: Lithium Quantification of Aged Lithium Ion Battery Graphite Electrodes by Means of Laser Ablation Inductively Coupled Plasma Mass Spectrometry and Inductively Coupled Plasma Optical Emission Spectroscopy. *J. Power Sources* **2017**, *356*, 47-55.

(32) Wan, C.; Xu, S.; Hu, M. Y.; Cao, R.; Qian, J.; Qin, Z.; Liu, J.; Mueller, K. T.; Zhang, J.-G.; Hu, J. Z. Multinuclear NMR Study of the Solid Electrolyte Interface Formed in Lithium Metal Batteries. *ACS Appl. Mater. Interf.* **2017**, *9*, 14741-14748.

(33) Zaban, A.; Aurbach, D. Impedance Spectroscopy of Lithium and Nickel Electrodes in Propylene Carbonate Solutions of Different Lithium Salts a Comparative Study. *J. Power Sources* **1995**, *54*, 289-295.

(34) Lu, P.; Li, C.; Schneider, E. W.; Harris, S. J. Chemistry, Impedance, and Morphology Evolution in Solid Electrolyte Interphase Films During Formation in Lithium Ion Batteries. *J. Phys. Chem. C* **2014**, *118*, 896-903.

(35) Kang, J.-H.; Kwak, W.-J.; Aurbach, D.; Sun, Y.-K. Sodium Oxygen Batteries: One Step Further with Catalysis by Ruthenium Nanoparticles. *J. Mat. Chem. A* **2017**, *5*, 20678-20686.

(36) Wang, H.-H.; Lee, Y. J.; Assary, R. S.; Zhang, C.; Luo, X.; Redfern, P. C.; Lu, J.; Lee, Y. J.; Kim, D. H.; Kang, T.-G.; Indacochea, E.; Lau, K. C.; Amine, K.; Curtiss, L. A. Lithium Superoxide Hydrolysis and Relevance to Li–O_2 Batteries. *J. Phys. Chem. C* **2017**, *121*, 9657-9661.

(37) Zhai, D.; Wang, H.-H.; Yang, J.; Lau, K. C.; Li, K.; Curtiss, L. A.; Amine, K. Disproportionation in Li-O_2 Batteries Based on Large Surface Area Carbon Cathode. *J. Am. Chem. Soc.* **2013**, *135*, 15364–15372.

(38) Hartmann, P.; Bender, C. L.; Sann, J.; Durr, A. K.; Jansen, M.; Janek, J.; Adelhelm, P. A Comprehensive Study on the Cell Chemistry of the Sodium Superoxide (NaO_2) Battery. *Phys. Chem. Chem. Phys.* **2013**, *15*, 11661-11672.

(39) Lu, J.; Jung Lee, Y.; Luo, X.; Chun Lau, K.; Asadi, M.; Wang, H.-H.; Brombosz, S.; Wen, J.; Zhai, D.; Chen, Z.; Miller, D. J.; Sub Jeong, Y.; Park, J.-B.; Zak Fang, Z.; Kumar, B.; Salehi-Khojin, A.; Sun, Y.-K.; Curtiss, L. A.; Amine, K. A Lithium–Oxygen Battery Based on Lithium Superoxide. *Nature* **2016**, *529*, 377-382.

(40) McCloskey, B. D.; Valery, A.; Luntz, A. C.; Gowda, S. R.; Wallraff, G. M.; Garcia, J. M.; Mori, T.; Krupp, L. E. Combining Accurate O_2 and Li_2O_2 Assays to Separate Discharge and Charge Stability Limitations in Nonaqueous Li–O_2 Batteries. *J. Phys. Chem. Lett.* **2013**, 2989-2993.

(41) Mahne, N.; Schafzahl, B.; Leypold, C.; Leypold, M.; Grumm, S.; Leitgeb, A.; Strohmeier, G. A.; Wilkening, M.; Fontaine, O.; Kramer, D.; Slugovc, C.; Borisov, S. M.; Freunberger, S. A. Singlet Oxygen Generation as a Major for Parasitic Reactions During Cycling of Aprotic Lithium-Oxygen Batteries. *Nat. Energy* **2017**, *2*, 17036.

(42) Schafzahl, L.; Mahne, N.; Schafzahl, B.; Wilkening, M.; Slugovc, C.; Borisov, S. M.; Freunberger, S. A. Singlet Oxygen During Cycling of the Aprotic Sodium–O_2 Battery. *Angew. Chem. Int. Ed.* **2017**, *56*, 15728-15732.

(43) Mahne, N.; Fontaine, O.; Thotiyl, M. O.; Wilkening, M.; Freunberger, S. A. Mechanism and Performance of Lithium-Oxygen Batteries - a Perspective. *Chem. Sci.* **2017**, *8*, 6716-6729.

(44) Wiberg, N.; Holleman, A. F.; Wiberg, E. Inorganic Chemistry; Academic Press: San Diego, USA; 2001.

(45) Kunze, U. R.; Schwedt, G. Grundlagen der Quantitativen Analyse; Wiley: Weinheim, Germany; 2009.

(46) Giordani, V.; Freunberger, S. A.; Bruce, P. G.; Tarascon, J.-M.; Larcher, D. H_2o_2 Decomposition Reaction as Selecting Tool for Catalysts in Li-O_2 Cells. *Electrochem. Solid State Lett.* **2010**, *13*, A180-A183.

(47) Meini, S.; Piana, M.; Tsiouvaras, N.; Garsuch, A.; Gasteiger, H. A. The Effect of Water on the Discharge Capacity of a Non-Catalyzed Carbon Cathode for Li-O_2 Batteries. *Electrochem. Solid State Lett.* **2012**, *15*, A45-A48.

(48) Ren, X.; Lau, K. C.; Yu, M.; Bi, X.; Kreidler, E.; Curtiss, L. A.; Wu, Y. Understanding Side Reactions in K–O_2 Batteries for Improved Cycle Life. *ACS Appl. Mater. Interf.* **2014**, *6*, 19299-19307.

(49) De Laat, J.; Gallard, H. Catalytic Decomposition of Hydrogen Peroxide by Fe(Iii) in Homogeneous Aqueous Solution: Mechanism and Kinetic Modeling. *Environ. Sci. Technol.* **1999**, *33*, 2726-2732.

(50) Duesterberg, C. K.; Mylon, S. E.; Waite, T. D. Ph Effects on Iron-Catalyzed Oxidation Using Fenton's Reagent. *Environ. Sci. Technol.* **2008**, *42*, 8522-8527.

Supplementary information

Quantifying Total Superoxide, Peroxide and Carbonaceous Compounds in Metal-O_2 Batteries and the Solid Electrolyte Interface

Bettina Schafzahl,[†] Eléonore Mourad,[†] Lukas Schafzahl,[†] Yann K. Petit,[†] Anjana R. Raju,[†,‡] Musthafa Ottakam Thotiyl,[‡] Martin Wilkening,[†] Christian Slugovc,[†] Stefan A. Freunberger*[,†]

[†]Institute for Chemistry and Technology of Materials, Graz University of Technology, Stremayrgasse 9, 8010 Graz, Austria

[‡]Department of Chemistry, Indian Institute of Science Education and Research (IISER) Pune, Dr. Homi Bhabha Road, Pashan, Pune, 411008, India

* Corresponding Author: freunberger@tugraz.at

Materials and Methods:

Chemicals

Ethylene glycol dimethyl ether (DME, >99.0%), diethylene glycol dimethyl ether (DEGDME, >99 %) and sodium trifluoromethanesulfonate (NaOTf, >98 %), were purchased from TCI EUROPE. Tetraethylene glycol dimethyl ether (tetraglyme, TEGDME, ≥99%) and $LiClO_4$ (battery grade, dry, 99.99%) were purchased from Sigma-Aldrich. Formic acid (puriss. ~98%) was bought from Fluka Analytical. Acetonitrile (HiPerSolv CHROMANORM Prolabo) was purchased from VWR Chemicals. Graphite and conductive carbon (SuperC65) were purchased from Timcal. Polyvinylidene difluoride (PvdF) was purchased from Arkema. N-methylpyrrolidone (NMP) was purchased from abcr. $LiNi_{0.8}Co_{0.15}Al_{0.05}O_2$ (NCA) was purchased from Ecopro. High purity oxygen (O_2 3.5, >99.95 vol %), high purity Ar (Ar 5.0, >99.999 vol %) and a mixture of Ar 6.0 and O_2 5.5 (Ar 5.01 vol%) were purchased from Messer Austria GmbH. Moisture determination of solvents and electrolytes according to Karl Fischer titration was performed on a TitroLine KF trace (Schott Instruments). Solvents were purified by distillation and further dried over activated molecular sieves. $LiClO_4$ was dried under vacuum for 24 h at 160 °C. All other chemicals were used without further purification. Li_2O_2 was synthesized

according to a previously reported procedure[1]. Li alkylcarbonates and α-MnO_2 nanowires were synthesized as reported previously.[2] Water was obtained from a Millipore purification unit.

Mass Spectrometry

The MS setup was built in-house and is similar to the one described previously.[3] It consisted of a commercial quadrupole mass spectrometer (Balzers) with a turbomolecular pump (Pfeiffer), which is backed by a membrane pump and leak inlet, which samples from the purge gas stream. The setup was calibrated for different gases (Ar, O_2, CO_2, H_2, N_2 and H_2O) using calibration mixtures in steps over the anticipated concentration ranges to capture nonlinearity and cross-sensitivity. All calibrations and quantifications were performed using in-house software written in MATLAB. The purge gas system consisted of a digital mass flow controller (Bronkhorst) and stainless steel tubing.

The sample setup consists of a glass vial with a volume of 7 mL equipped with a small stirring bar. A PEEK plug with glued in PEEK tubes and an exchangeable septum is sealed against the glass vial with a flat silicone rubber seal, which are all pressed by an Al clamp. During the measurement, the solutions are added through a septum using a syringe and the gas flow is regulated using a four way valve. The gas flow is fixed to 5 mL per minute. Before the measurement is started, all solutions were degassed with N_2 for at least 15 minutes to remove dissolved CO_2 and O_2.

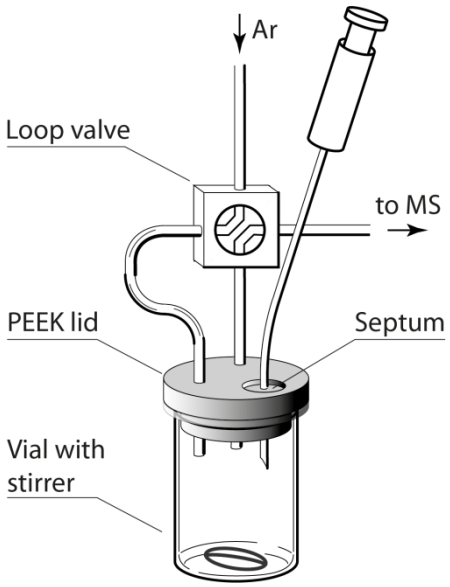

Figure S1. Schematic of the sample setup consisting of vial with stirrer, PEEK lid with septum, purge tubing with a loop valve and a syringe.

Electrode Fabrication and Cell Design

Li–O_2 cathodes were made from a slurry of Super P carbon black (TIMCAL) with PTFE (60% dispersion in H_2O, Aldrich) binder in the ratio 9:1 (m/m) using isopropanol. The slurry was then coated onto a stainless steel mesh current collector. The electrodes were vacuum dried at 120 °C for 24 h and then transferred to an Ar filled glove box without exposure to air. For the Na–air cells, carbon paper cathodes (Freudenberg H2315) were heated to 900 °C under Ar/H_2 (95/5 vol/vol) atmosphere. The glass fiber separators (Whatman) were washed with ethanol and dried overnight at 170 °C under vacuum prior to use. The $LiFePO_4$ counter electrodes were made by mixing partially delithiated active material with Super P and PTFE in the ratio 8:1:1(m/m/m). The electrodes were vacuum dried at 120 °C for 24 h. The counter electrode had three-fold the expected capacity of the positive electrode. The electrochemical cells used to investigate cycling were based on a Swagelok design. Typical Li-O_2 working electrodes had a carbon mass loading of 1 mg and the cells were assembled with 100 µL electrolyte. Li-O_2 cells comprised a Super P/PTFE working electrode, $Li_{1-x}FePO_4$ reference and counter electrodes and 0.1M $LiClO_4$ in tetraglyme as the electrolyte and were run at 70 $mA \cdot g_C^{-1}$. Na-O_2 cells comprised a carbon paper working electrode, Na metal reference and counter electrodes and 0.1M NaOTf in diglyme containing 40 ppm H_2O as the electrolyte and were run at 90 $\mu A \cdot cm^{-2}$.

For Li-ion cells, graphite anodes were prepared from a slurry of 83% graphite, 8.5% conductive carbon and 8.5% polyvinylidene difluoride in NMP. NCA cathodes were prepared from a slurry of 84% NCA, 8% PvdF and 8% conductive carbon. Both slurries were stirred overnight, sonicated and cast on a Cu and Al foil, respectively. Subsequently, electrodes were punched and dried at 120 °C under vacuum. The average loading was roughly 1 mg cm^{-2} for graphite anodes and roughly 3 mg cm^{-2} for NCA cathodes.

Electrochemical tests were run on either a SP-300 (BioLogic SA, France) or BT-2000 (Arbin Instruments) potentiostat/galvanostat. For the analysis of the electrodes, batteries were, after cycling, disassembled in an argon filled glovebox without exposure to air. If not noted otherwise, all electrodes were washed and dried before measuring. DMC (metal-ion batteries) or DME (metal-air cells) were used for that purpose and the solvent was subsequently removed under reduce pressure. The washing/drying step was done within one hour after the cells were finished.

Spectroscopic Methods

UV-Vis Spectroscopy

Absorption spectra were recorded on a UV-Vis spectrophotometer (Varian Cary 50). 2 wt% solution of Ti(IV)-oxysulfate solution in 1 M H_2SO_4 was used for the detection of peroxides except for data in

Fig. 1 where 2 % Ti(IV)-oxysulfate solution in 0.1 M H_2SO_4 was used as reported earlier.[4,5] The absorbance at the maximum at 405 nm was chosen for all measurements.

Calibrating UV-Vis absorbance with H_2O_2 is prone to yield a curve that does not pass through zero, i.e. due to loss of H_2O_2.[4] To obtain the true H_2O_2 concentration, we thus started from high purity Li_2O_2 and accounted for any H_2O_2 loss by measuring evolved O_2 with the MS, Fig. S6.

Supplementary Discussion and Figures:

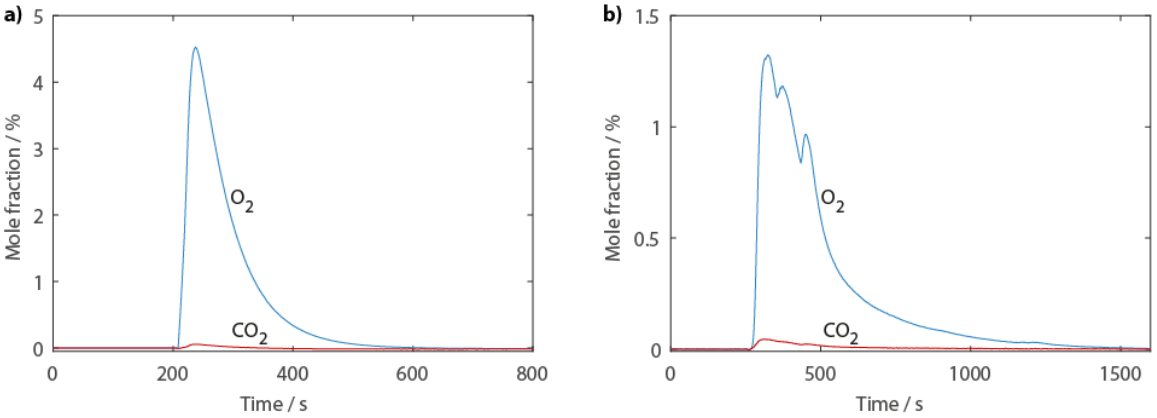

Figure S2. CO_2 evolution indicates reactive species upon expelling O_2 from H_2O_2. In either case the H_2O_2 source was Li_2O_2 and Li acetate was used as organic probe molecule. a) A mixture of Li_2O_2 /CH_3COOLi (90/10 wt.%) was mixed with an equal amount of α-MnO_2 nanowires and immersed in 1 M H_2SO_4 solution. The CO_2 amount corresponds to ~10% of the CH_3COOLi to be decomposed. b) The Li_2O_2/CH_3COOLi mixture was immersed in 0.5 M $FeCl_3$ solution. The CO_2 amount corresponds to ~12% of the CH_3COOLi to be decomposed.

Quantifying total peroxide/superoxide by total O_2 evolution

Fe^{3+} decomposes H_2O_2 catalytically for which either the Kremer-Stein-Mechanism

$$Fe^{3+} \overset{\pm H_2O_2}{\longleftrightarrow} Fe^{III}(O_2H_2)^{3+} \overset{\pm H_2O}{\longleftrightarrow} Fe^{V}O^{3+} \overset{\pm H_2O_2}{\longleftrightarrow} Fe^{III}(O_3H_2)^{3+} \rightarrow Fe^{3+} + O_2 + H_2O \qquad (S1)$$

or other mechanisms involving $HO_2^{\bullet}$ or $^{\bullet}OH$ were proposed.[6,7] Fe^{3+} decomposes H_2O_2 quantitatively as shown in Table S1 for various Fe^{3+}–to–Li_2O_2 ratios and in Fig. S3 for different amounts of Li_2O_2.

Table S1. Oxygen yield for various Fe^{3+}–to–Li_2O_2 ratios.

Fe^{3+} concentration (M)	Fe^{3+}–to–Li_2O_2 ratio	O_2 yield (%)
0.05	0.2/1	96
0.1	0.6/1	100
0.5	2.5/1	99
1	4/1	101

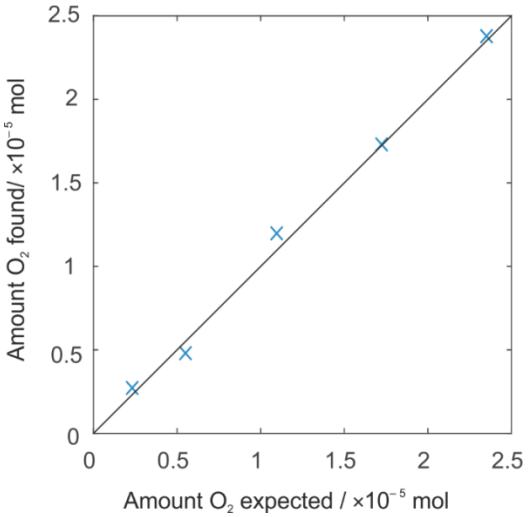

Figure S3. Comparison of the amount of Li_2O_2 used and O_2 evolved using 0.1 M $FeCl_3$. Linear regression gives $n_{O_2,found} = 1.015 \cdot n_{O_2,expected}$ with $R^2 = 0.9948$.

Quantifying total peroxide/superoxide by combining MS and UV-Vis

Superoxide and peroxide are quantified by combining photometry of the $[Ti(O_2)OH]^+$ complex[7] and MS measurement of the O_2 evolved during sample preparation as shown in Fig. 2a-c. We first consider the case that the discharge product is either Li_2O_2, Na_2O_2, NaO_2, or KO_2, but no mixtures thereof. When M_2O_2 is measured, acidifying the sample will convert the Li_2O_2 according to

$$\mathrm{M_2O_2 + 2\,H_2O \rightarrow H_2O_2 + 2\,MOH} \qquad \text{(S2)}$$

while part of the H_2O_2 will decompose into H_2O and O_2 according to

$$\mathrm{H_2O_2 \rightarrow H_2O + \frac{1}{2}\,O_2} \qquad \text{(S3)}$$

Thus any one mole O_2 evolved corresponds to 2 moles M_2O_2, which are not any more present as H_2O_2 and therefore not captured by UV-Vis. One mole of H_2O_2 detected as $[Ti(O_2)OH]^+$ by UV-Vis correspond to one mole of M_2O_2. The moles of H_2O_2 and O_2 per mol of M_2O_2 as a function of the H_2O_2 loss into the gas phase are plotted in Fig. S4a.

With x being the fraction of H_2O_2 lost, the moles n of H_2O_2 and O_2 are

$$n_{\mathrm{H_2O_2}} = n_{\mathrm{M_2O_2}} - x \cdot n_{\mathrm{M_2O_2}} \qquad \text{(S4)}$$

$$n_{\mathrm{O_2}} = 0.5x \cdot n_{\mathrm{M_2O_2}} \qquad \text{(S5)}$$

Thus moles of Li_2O_2 are

$$\boldsymbol{n_{\mathrm{M_2O_2}} = n_{\mathrm{H_2O_2}} + 2 \cdot n_{\mathrm{O_2}}} \qquad \textbf{(S6)}$$

When NaO_2 or KO_2 is measured, acidifying the sample will convert the MO_2 according to

$$\mathrm{2\,MO_2 + 2\,H_2O \rightarrow H_2O_2 + O_2 + 2\,MOH} \qquad \text{(S7)}$$

while again part of the H_2O_2 will decompose into H_2O and O_2 according to Eq. S3. With x being the fraction of H_2O_2 lost, the moles of H_2O_2 and O_2 are

$$n_{H_2O_2} = 0.5 \cdot n_{MO_2} - 0.5x \cdot n_{MO_2} \quad \text{(S8)}$$

$$n_{O_2} = 0.5 \cdot n_{MO_2} + 0.25x \cdot n_{MO_2} \quad \text{(S9)}$$

Thus the moles of MO_2 are

$$\boldsymbol{n_{MO_2} = \frac{4}{3}\left(n_{O_2} + \frac{1}{2} \cdot n_{H_2O_2}\right)} \quad \textbf{(S10)}$$

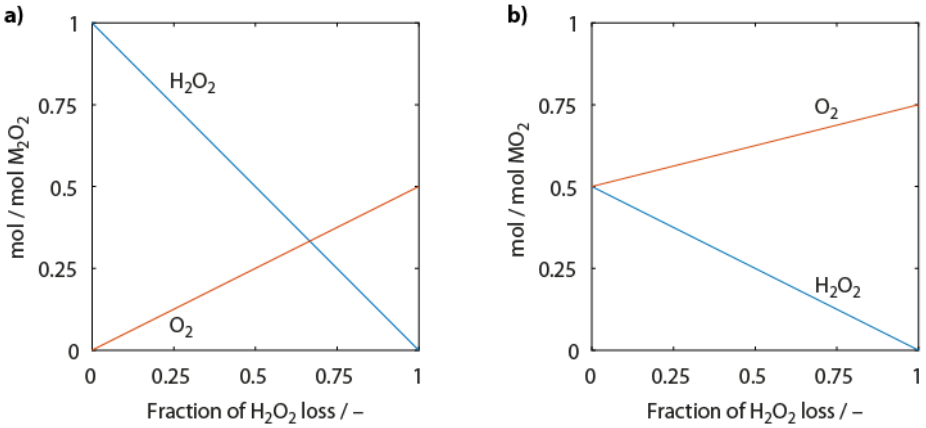

Figure S4. Amount of O_2 in the gas phase and H_2O_2 in the solution as a function of the fraction of theoretical amount of H_2O_2 lost into the gas phase for (a) M_2O_2 as given in Eq. S4 and S5, and (b) NaO_2 or KO_2 as given in Eq. S8 and S9.

When mixtures of MO_2 and M_2O_2 (M = Li or Na) are expected, two cases need to be distinguished.

I) LiO_2 decomposes according to

$$4\ LiO_2 + 2\ H_2O \rightarrow 3\ O_2 + 4\ LiOH \quad \text{(S11)}$$

without forming H_2O_2 while Li_2O_2 forms H_2O_2 via Eq. S2.[8] Since both the fraction x of H_2O_2 being lost and the Li_2O_2-to-LiO_2 ratio are unknowns, n_{Li^+} needs to be obtained as a third measure next to $n_{H_2O_2}$ and n_{O_2}. According to Equations S2, S3, and S11 these measures are are connected to $n_{Li_2O_2}$ and n_{LiO_2} via

$$n_{H_2O_2} = n_{Li_2O_2} - x \cdot n_{Li_2O_2} \quad \text{(S12)}$$

$$n_{O_2} = 0.5x \cdot n_{Li_2O_2} + \frac{4}{3} \cdot n_{LiO_2} \quad \text{(S13)}$$

$$n_{Li^+} = 2\ n_{Li_2O_2} + n_{LiO_2} \quad \text{(S14)}$$

These quantities are plotted as a function of LiO_2 mole fraction in Fig. S7a for various values of H_2O_2 loss x. The moles of Li_2O_2 and LiO_2 are then obtained via

$$\boldsymbol{n_{Li_2O_2} = \frac{6}{13}\left(\frac{4}{3} n_{Li^+} - \frac{1}{2} n_{H_2O_2} - n_{O_2}\right)} \quad \text{(S15)}$$

$$\boldsymbol{n_{LiO_2} = n_{Li^+} - 2n_{Li_2O_2}} \quad \text{(S16)}$$

II) NaO_2 decomposes according to

$$2\,NaO_2 + 2\,H_2O \rightarrow H_2O_2 + \,O_2 + \,2\,NaOH \qquad \text{(S7)}$$

thus forming H_2O_2.[8] Na_2O_2 forms H_2O_2 via Eq. S2. Since both the fraction x of H_2O_2 being lost and the Na_2O_2-to-NaO_2 ratio are unknowns, n_{Na^+} needs to be obtained as a third measure next to $n_{H_2O_2}$ and n_{O_2}. According to Equations S2, S3, and S7 these measures are are connected to $n_{Na_2O_2}$ and n_{NaO_2} via

$$n_{H_2O_2} = n_{Na_2O_2} + \frac{1}{2}\cdot n_{NaO_2} - x\cdot n_{Na_2O_2} + \frac{x}{2}\cdot n_{NaO_2} \qquad \text{(S17)}$$

$$n_{O_2} = \frac{x}{2}\cdot n_{Na_2O_2} + \frac{1}{2}\cdot n_{NaO_2} + \frac{x}{4}\cdot n_{NaO_2} \qquad \text{(S18)}$$

$$n_{Na^+} = 2\,n_{Na_2O_2} + \,n_{NaO_2} \qquad \text{(S19)}$$

These quantities are plotted as a function of LiO_2 mole fraction in Fig. S7b for various values of H_2O_2 loss x. The moles of Na_2O_2 and NaO_2 are then obtained via

$$\boldsymbol{n_{Na_2O_2} = \frac{3}{4}n_{Na^+} - \frac{1}{2}n_{H_2O_2} - n_{O_2}} \qquad \text{(S20)}$$

$$\boldsymbol{n_{NaO_2} = n_{Na^+} - 2n_{Na_2O_2}} \qquad \text{(S21)}$$

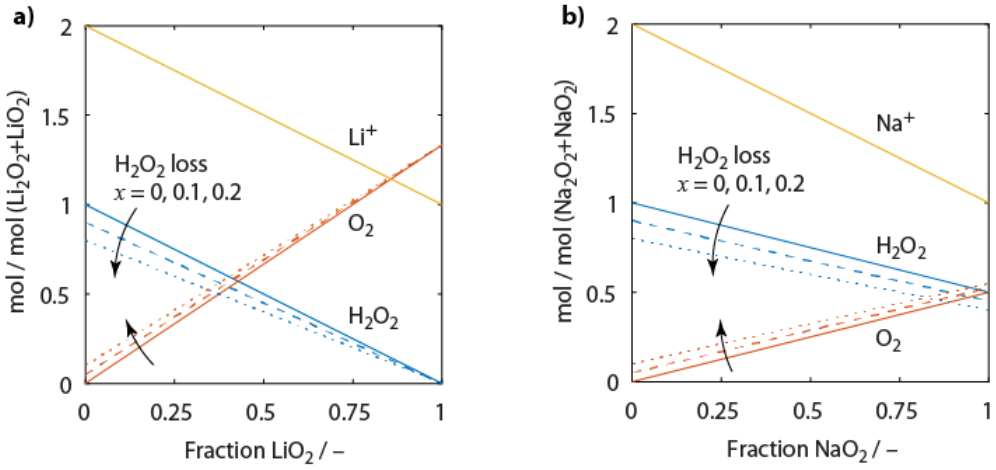

Figure S5. Analysis of mixtures of MO_2 and M_2O_2 (M = Li or Na). Amount of O_2 in the gas phase and H_2O_2 and M^+ in the solution as a function of the mole fraction of superoxide in the mixture. In either case the effect of a H_2O_2 loss of 0, 10, 20% (*i.e.*, x = 0, 0.1, 0.2) into the gas phase is examined. (a) Analysis of LiO_2/Li_2O_2 mixtures as given in Eq. S12, S13 and S14. (b) Analysis of NaO_2/Na_2O_2 mixtures as given in Eq. S17, S18 and S19.

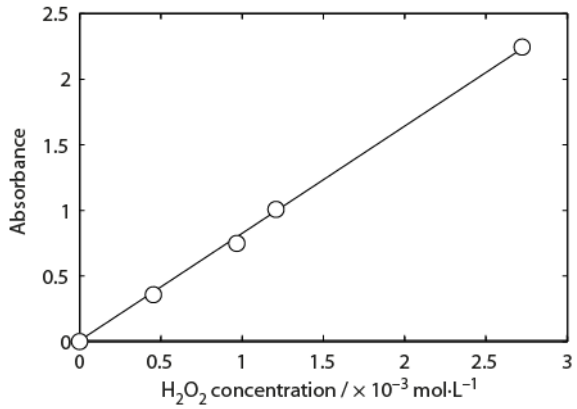

Figure S6. Calibration curve for UV-Vis absorbance vs. true H_2O_2 concentration. Linear regression gives $A = 819.84 \cdot c_{H_2O_2}$ with $R^2 = 0.9992$.

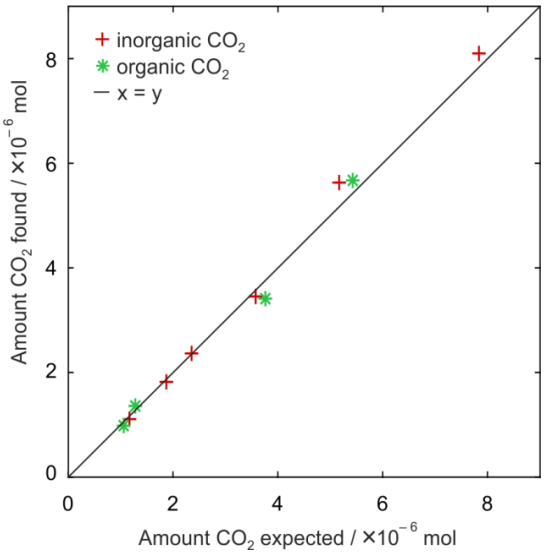

Figure S7. Detection accuracy for inorganic and organic carbonaceous compounds. Mechanical mixtures of Li_2CO_3 and Li acetate were analyzed using the protocol shown in Fig. 2. Linear regression gives for the inorganic CO2 $n_{CO_2,found} = 1.033 \cdot n_{CO_2,expected}$ with $R^2 = 0.9954$ and for the organic CO_2 $n_{CO_2,found} = 0.999 \cdot n_{CO_2,expected}$ with $R^2 = 0.986$.

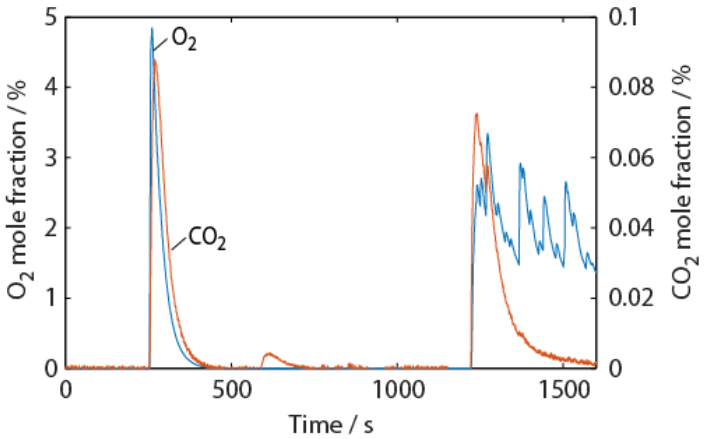

Figure S8. Exemplary MS data for measuring a discharged Na–O_2 cathode.

Supplementary References

(1) Ottakam Thotiyl, M. M.; Freunberger, S. A.; Peng, Z.; Bruce, P. G. The Carbon Electrode in Nonaqueous Li–O_2 Cells. *J. Am. Chem. Soc.* **2013**, *135*, 494-500.

(2) Freunberger, S. A.; Chen, Y.; Peng, Z.; Griffin, J. M.; Hardwick, L. J.; Bardé, F.; Novák, P.; Bruce, P. G. Reactions in the Rechargeable Lithium–O_2 Battery with Alkyl Carbonate Electrolytes. *J. Am. Chem. Soc.* **2011**, *133*, 8040-8047.

(3) Chen, Y.; Freunberger, S. A.; Peng, Z.; Bardé, F.; Bruce, P. G. Li–O_2 Battery with a Dimethylformamide Electrolyte. *J. Am. Chem. Soc.* **2012**, *134*, 7952-7957.

(4) Hartmann, P.; Bender, C. L.; Sann, J.; Durr, A. K.; Jansen, M.; Janek, J.; Adelhelm, P. A Comprehensive Study on the Cell Chemistry of the Sodium Superoxide (NaO_2) Battery. *Phys. Chem. Chem. Phys.* **2013**, *15*, 11661-11672.

(5) Meini, S.; Piana, M.; Tsiouvaras, N.; Garsuch, A.; Gasteiger, H. A. The Effect of Water on the Discharge Capacity of a Non-Catalyzed Carbon Cathode for Li-O_2 Batteries. *Electrochem. Solid State Lett.* **2012**, *15*, A45-A48.

(6) De Laat, J.; Gallard, H. Catalytic Decomposition of Hydrogen Peroxide by Fe(III) in Homogeneous Aqueous Solution: Mechanism and Kinetic Modeling. *Environ. Sci. Technol.* **1999**, *33*, 2726-2732.

(7) Wiberg, N.; Holleman, A. F.; Wiberg, E. Inorganic Chemistry; Academic Press: San Diego, USA; 2001.

(8) Wang, H.-H.; Lee, Y. J.; Assary, R. S.; Zhang, C.; Luo, X.; Redfern, P. C.; Lu, J.; Lee, Y. J.; Kim, D. H.; Kang, T.-G.; Indacochea, E.; Lau, K. C.; Amine, K.; Curtiss, L. A. Lithium Superoxide Hydrolysis and Relevance to Li–O_2 Batteries. *J. Phys. Chem. C* **2017**, *121*, 9657-9661.